SCIENCE CHINA
Technological Sciences

Special Topic: Nonlinear Dynamics and Control
•Article•

August 2022 Vol.65 No.8: 1661–1674
https://doi.org/10.1007/s11431-021-2066-7

# Energy-efficient firing modes of chay neuron model in different bursting kinetics

LU LuLu*, YI Ming & LIU XiaoQian

*School of Mathematics and Physics, China University of Geosciences, Wuhan 430074, China*

Received December 29, 2021; accepted April 22, 2022; published online July 26, 2022

The firing sequence of the neuron system that transmits information consumes a significant amount of energy, but it is unclear how the firing pattern of the neuron system determines its energy efficiency. The mode transformation and energy efficiency in different firing modes are investigated using the Chay neuron model. It has been found that when system parameters are tuned, the neurons show complex bursting kinetics. The period-*n* bursting state of the neuron carries high amounts of information while consuming less energy per unit of information, resulting in higher energy efficiency. In particular, the mixed discharge state, where the neuron is in several bursting states simultaneously, is more energy efficient, and appropriate electromagnetic inductioncan enhance the neuron's energy efficiency. Furthermore, there are optimal system parameters that maximize the energy efficiency of firing modes, demonstrating that the neuron carries high amounts of information while consuming less energy per unit of information. The study helps to understand the energy mechanism of neural information propagation and provides an insight into the energy efficiency characteristic of neuron systems.

**energy efficiency, firing modes, bursting kinetics, electromagnetic induction**

**Citation:** Lu L L, Yi M, Liu X Q. Energy-efficient firing modes of chay neuron model in different bursting kinetics. Sci China Tech Sci, 2022, 65: 1661–1674, https://doi.org/10.1007/s11431-021-2066-7

## 1 Introduction

A neuron is the basic unit of information processing in the neurological system [1,2]. Neurons consume ten times the energy of body cells. The human brain consumes more than 20% of the body's energy but weighs only 2% of the body. Neurons compute and communicate primarily through action potentials and synaptic potentials [3,4]. In neurons, synaptic activity consumes 60% of the energy, action potential consumes 10%, and resting metabolism consumes 30%.

The neural system is important, multidimensional, and complex, and each neuron has a unique firing mode, information processing mode, and information coding mode [5–7]. Thus, it is necessary to construct the nervous system using biological, physical, and mathematical methods based on key neural circuits and microneural networks and to study the effects of intrinsic and extrinsic factors on the complex neuron system's nonlinear dynamic characteristics through stochastic simulation and nonlinear dynamic analysis [8–12].

Numerous elements influence the dynamic behavior of neuron systems, such as fluctuation or randomness, internal and external stimuli, energy transitions, time delay, and electromagnetic radiation [13–18]. Neurons show a variety of discharge behaviors under various conditions, such as periodic spike discharge mode, period-doubling cluster discharge mode, and mixed discharge mode [19]. These discharge states can also be observed in the experiment [20,21]. The firing sequence of the neuron system carries different amounts of information in various firing modes, and the information-carrying firing modes consume a significant amount of energy during the transition phase [22–24]. Because information coding occurs within a limited energy

*Corresponding author (email: lululu@cug.edu.cn)

range, the energy efficiency of neural information transmission is a necessary limiting factor for the neuron system [25,26]. Recent studies show that neural information is more likely to be encoded by sequences of spikes than by single spikes [27], and energy efficiency depends not only on a single peak but also on the state of the discharge mode.

There are many methods of analyzing neural coding, but two of the most important are the principle of minimum mutual information and the principle of maximum entropy [28–30]. In the case of minimum mutual information, energy consumption is minimal, and the amount of information obtained is also minimal. At the same time, the energy consumed in obtaining the maximum entropy is very large, as is the information obtained. In addition, Hamilton energy [31–33] is used to estimate the dependency of states on energy in the oscillator model and neuron using Helmholtz's theorem.

High energy consumption implies that the neural system must operate efficiently, showing that neurons must process as much information as possible with the lowest energy consumption [34–36]. And because the human brain is relatively efficient, this is considered an important principle for the nervous system's evolution under selective pressure [37]. There are many studies on energy; for example, a neural energy calculation method was proposed for calculating the power of neuron bursts with or without current stimulation, and it was found that neurons consume the least energy in the bursting state [38]. The reference [39] discussed brain energy metabolism in detail, with an emphasis on the metabolic interactions between neurons and astrocytes. The energy and collective dynamics were studied in the model of the star-coupled neuron [40] and were found to be applicable to the same and different chaotic oscillator networks.

In addition, an energy factor was proposed to measure the metabolic demand during neuronal discharge, and it was found that excitatory neurons consume more energy during pathological seizures than they do during normal firing mode, whereas inhibitory neurons consume less energy to enter the seizure process than excitatory neurons do during normal firing mode [41]. The reference [42] adopted the energy cost theory to distinguish epileptiform discharges from normal spike discharges and observed that the transition of somatic discharge patterns from regular to epileptiform discharges coexisted with "energy explosions," i.e., epileptiform discharges consume more energy than conventional discharges.

Additionally, some researchers studied the energy of the neuron system from the perspective of circuits and biological experiments [43–48]. The VLSI circuit was developed to study the energy consumption of leaky integrate and fire neurons, as well as to implement hardware acceleration [43]. It is found through experiments that fast Cordic-based Izhikevich neurons have higher energy efficiency and accuracy than traditional Cordic-based designs [45]. Integrated circuits based on ultra-low energy bionic neurons and synapses have been demonstrated [47], and neurons and synapses using STDP circuits consume low energy. The biological experiment [48] used biological data analysis to evaluate the relationship between neuron-astroglia metabolic rate and volume fraction. An experimental study [49] of non-myelinated mossy fibers of the rat hippocampus found that the less temporal overlap of inward $Na^+$ and outward $K^+$ currents during action potentials, the lower the energy cost and the higher the energy efficiency. In addition, the reference [50] analyzed intracranial EEG recordings of patients and found that neuronal firing becomes more common and cumulative energy increases prior to seizure.

Although extensive research has been conducted on the energy supply and consumption of neuron systems [37,51,52], surprisingly little attention has been devoted to the relationship between energy efficiency and complex firing modes. In particular, combining information and energy shows the inner connection between neural information and neural energy. As a result, an interesting question now arises: How does the nervous system's firing pattern determine energy efficiency? How does electromagnetic induction affect the supply and consumption of energy by neurons? How do the tuning system parameters affect the neuron's energy efficiency?

To address these challenges, we investigate the energy-efficient firing modes associated with different bursting kinetics using the Chay neuron model. Section 2 introduces the neural model and the formula for energy consumption and energy efficiency. Section 3 discusses complex firing modes and their transformations, followed by the study of the impact of control parameters (relaxation time constants $\lambda_n$, maximal conductances $g_{kc}$, and feedback gains $k$) on energy consumption and efficiency. It has been found that there are optimal system parameters where the energy efficiency of firing modes is greatest, and the neuron carries high amounts of information while consuming less energy per unit of information. This discovery has significant implications for understanding the different coding patterns found in the neuron system.

## 2 Model and methods

### 2.1 The Chay neuron model

The Chay neuron model is a unified new theoretical model based on many different types of excitable cells, such as neurons, cardiomyocytes, and sensory terminals, that are related to $Ca^{2+}$ ions and play an important role in $K^+$ ion channels. This model can simulate various periodic, quasi-periodic, and chaotic cluster discharge and spike discharge rhythm patterns of real excitatory cells [25,53]. The mem-

brane potential dynamics of the improved Chay neuron model is

$$\frac{dV}{dt} = -I_{kv} - I_{kc} - I_i - I_l - I_\varphi, \tag{1}$$

$$\frac{dC}{dt} = \rho(m_\infty^3 h_\infty (V_C - V) - k_C C), \tag{2}$$

$$\frac{dn}{dt} = \lambda_n (n_\infty - n)(\alpha_n + \beta_n), \tag{3}$$

$$\frac{d\varphi}{dt} = k_1 V - k_2 \varphi, \tag{4}$$

where $V$ is membrane potential, $C$ is the intracellular $Ca^{2+}$ concentration, $n$ is the probability of opening a voltage-dependent $K^+$ channel, and $\varphi$ is magnetic flux, which describes the influence of electromagnetic induction. $\rho$ is the proportionality constant, $\lambda_n$ is the relaxation time constant, $V_C$ is the reversal potential for $Ca^{2+}$ ions, and $k_C$ is the ratio constant of intracellular $Ca^{2+}$ ions.

The term $I_{kv}$ is the ionic current of the outward voltage-dependent $K^+$, $I_{kc}$ is the ionic current of the outward calcium-dependent $K^+$, $I_i$ is the ionic current of the inward mixed $Na^+$-$Ca^{2+}$, and $I_l$ is the leakage current [25]. The term $I_\varphi$ is the feedback current on the membrane potential caused by electromagnetic induction. Their descriptions are

$$I_{kv} = g_{kv} n^4 (V - V_k), \tag{5}$$

$$I_{kc} = g_{kc} \frac{C}{1+C} (V - V_k), \tag{6}$$

$$I_i = g_i m_\infty^3 h_\infty (V - V_i), \tag{7}$$

$$I_l = g_l (V - V_l), \tag{8}$$

$$I_\varphi = k(a + 3b\varphi^2)(V - V_\varphi), \tag{9}$$

where $g_{kv}$, $g_{kc}$, $g_i$, and $g_l$ are the maximal conductances, $V_k$, $V_i$, $V_l$, $V_C$, and $V_\varphi$ are reversal potentials. Parameter $k$ is feedback gain, and the electromagnetic induction intensity depends on the value of two parameters ($k$, $k_1$). $m_\infty$ and $h_\infty$ are activation and deactivation probabilities of the mixed channel, and $n_\infty$ is the steady-state value:

$$y_\infty = \frac{\alpha_y}{\alpha_y + \beta_y}, y = m, h, n, \tag{10}$$

$$\alpha_m = \frac{0.1(25+V)}{(1 - e^{-0.1V-2.5})}, \ \beta_m = 4e^{-(V+50)/18}, \tag{11}$$

$$\alpha_h = 0.07e^{-0.05V-2.5}, \ \beta_h = \frac{1}{(1+e^{-0.1V-2})}, \tag{12}$$

$$\alpha_n = \frac{0.01(20+V)}{(1 - e^{-0.1V-2})}, \ \beta_n = 0.125e^{-(V+30)/80}, \tag{13}$$

where $\alpha_n$ and $\beta_n$ are the opening and closing rates of the $K^+$ channel, $\alpha_m$ and $\beta_m$ are the opening and closing rates of the $Na^+$ channel activation gates, respectively, $\alpha_h$ and $\beta_h$ are the opening and closing rates of the $Na^+$ channel deactivation gates, respectively.

The values of parameters are set as $V_k$ = −75 mV, $V_i$ = 100 mV, $V_l$ = −40 mV, $V_C$ = 100 mV, $V_\varphi$ = 16.0 mV, $g_i$ = 1800 $s^{-1}$, $g_{kv}$ = 1700 $s^{-1}$, $g_l$ = 7 $s^{-1}$, $\rho$ = 0.27 $mV^{-1}$ $s^{-1}$, $k_C$ = 3.3/18, $a$ = 0.4, $b$ = 0.02, and $k_1$ = 0.1 and $k_2$ = 0.1, the detailed explanation of these parameters can be viewed in refs. [52,54]. The Chay neuron model has a basic assumption [53,55] that the potential energy stored in the battery reverse potentials $V_i$, $V_l$, $V_k$, $V_\varphi$ in the circuit comes from the bioenergy ATP consumed by the Na/K-ATPase pump. The schematic diagram for the improved Chay neuron circuit is shown in Figure 1. The electric power provided by batteries $V_i$ and $V_\varphi$ makes the membrane potential less negative (depolarization), and the electric power provided by batteries $V_k$ and $V_l$ makes the membrane potential more negative. Furthermore, nonlinear equations are integrated by using Euler's algorithm, and the time step is 0.00001.

## 2.2 Energy consumption and energy efficiency

The energy estimation method proposed in previous studies [25,38] was adopted, and the net power $P(t)$ causing changes in membrane voltage is as follows:

$$P(t) = |I_k V_k| + |I_l V_l| - |I_i V_i| - |I_\phi V_\phi|, \tag{14}$$

where the rate at which each battery transfers electrical energy to the capacitor $C_m$ is its electrical current multiplied by its electromotive force $|I_y V_y|$ ($y$ = $i$, $k$, $l$, $\varphi$), and the corresponding net power $P$ during the action potential and its following hyperpolarization. When $P(t)$ is positive, the energy consumed to change the membrane potential comes from the electrical power of batteries $|I_k V_k| + |I_l V_l|$, which is not counterbalanced by the electrical power of batteries $|I_i V_i| + |I_\varphi V_\varphi|$, the positive energy is calculated during the time period $T$ (120 s) of the firing activities:

$$E_{\text{positive}} = \begin{cases} \int_0^T P(t)dt, & P \geq 0, \\ 0, & P < 0. \end{cases} \tag{15}$$

Simultaneously, when $P(t)$ is negative, electrical power

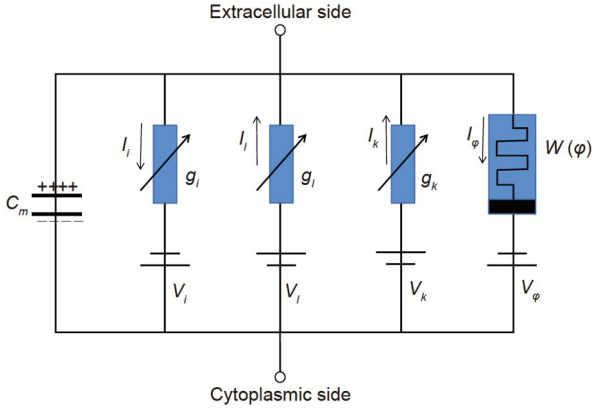


**Figure 1** (Color online) Schematic of neuron circuit under electromagnetic induction.

$|I_iV_i| + |I_\varphi V_\varphi|$ provides the energy consumed to change the membrane potential, which is not counterbalanced by battery electrical power $|I_kV_k| + |I_lV_l|$. The negative energy is calculated as follows:

$$E_{\text{negative}} = \begin{cases} 0, & P \geq 0, \\ \int_0^T -P(t)\mathrm{d}t, & P < 0, \end{cases} \tag{16}$$

so the total energy consumption ($E$) is

$$E = E_{\text{positive}} + E_{\text{negative}} = \int_0^T |P(t)|\,\mathrm{d}t. \tag{17}$$

The ratio ($\delta$) of the negative energy consumption to positive energy consumption is

$$\delta = \frac{E_{\text{negative}}}{E_{\text{positive}}}. \tag{18}$$

Each firing pattern is converted into a series of ISI (interspike intervals), the standard deviation ($\sigma$) and the mean ($\mu$) of which are given by

$$\sigma = \sqrt{\frac{1}{N}\sum_{n=1}^{N}(t_n - \mu)^2}, \tag{19}$$

$$\mu = \frac{1}{N}\sum_{n=1}^{N} t_n. \tag{20}$$

Therefore, the information (coefficient of variation, $CV$) of the spike sequence variation is given as

$$CV = \frac{\sigma}{\mu} = \frac{\sqrt{\frac{1}{N}\sum_{n=1}^{N}(t_n - \mu)^2}}{\frac{1}{N}\sum_{n=1}^{N} t_n}. \tag{21}$$

The more irregular the firing pattern is, the larger the value of the $CV$ is and, accordingly, the more information it carries. In addition, the value $\eta$ is calculated from energy consumption per unit of information as follows:

$$\eta = \frac{E}{CV} = \frac{\int_0^T |P(t)|\mathrm{d}t \cdot \frac{1}{N}\sum_{n=1}^{N} t_n}{\sqrt{\frac{1}{N}\sum_{n=1}^{N}(t_n - \mu)^2}}. \tag{22}$$

A smaller $\eta$ value means higher energy efficiency, i.e., lower energy consumption per unit of information. Correspondingly, a higher $\eta$ value means lower energy efficiency. In order to satisfy the statistical law, the $CV$ is calculated over a time length of 1200 s.

## 3 Results

### 3.1 Different bursting kinetics of the Chay neuron model

First, so as to show the complex firing modes of neurons, the bifurcation diagrams of ISI are plotted with the different parameters, as shown in Figure 2.

The electrical activities of the neuron show a series of firing modes transformation: as system parameters change, the firing mode transforms between spiking and bursting behaviors, with the bursting behavior including chaotic and periodic bursting states (such as period-2 state, …, 11, …, and even period-25 state).

As shown in Figure 2(a), as the time constant $\lambda_n$ increases, the dynamic transition experiences the following succession: spiking state → period-2 bursting state → period-3 bursting state → period-4 bursting state → period-$n$ bursting state → spiking state, and the $\lambda_n$ values for the critical point of the spiking and bursting state are 240 and 381, respectively. In Figure 2(b), as the $g_{kc}$ increases, the firing mode undergoes an interesting transformation: spiking state → chaos state → period-4 bursting state → period-3 bursting state → period-2 bursting state → closed spiking state. This presents an opposite trend to the firing mode transition with increasing time constant $\lambda_n$, and the $g_{kc}$ values for the critical point of the spiking and bursting state are 10.35 and 19.55, respectively. Furthermore, the complex bifurcation process of the feedback gain $k$ is period-2 bursting state → spiking state → period-2 bursting state → closed spiking state, and the $k$ values for the critical point of the four state transitions are 0.00112, 0.0115, and 0.0206. Compared with previous work [25], the discharge activity of neurons induced by electromagnetic induction is more complex, showing a mixed discharge state in which neurons are in several bursting states

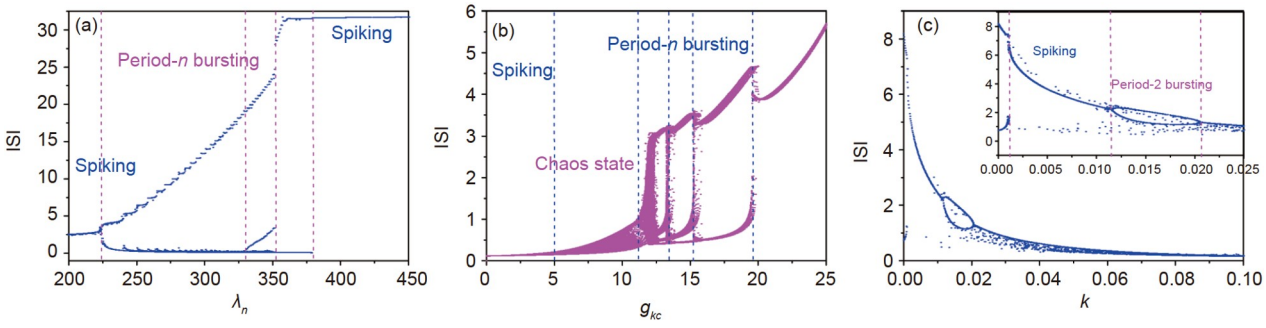


**Figure 2** (Color online) Dynamics of complex firing modes in the theoretical neuron model. Bifurcation diagrams with (a) various relaxation time constants $\lambda_n$ (the fixed parameters: $g_{kc} = 23.6\ \text{s}^{-1}$, $k = 0.001$), (b) various maximal conductances $g_{kc}$ (the fixed parameters: $\lambda_n = 230$, $k = 0.001$), and (c) various feedback gains $k$ (the fixed parameters: $\lambda_n = 240.4$, $g_{kc} = 23.6\ \text{s}^{-1}$).

simultaneously.

In addition, the neuronal diverse firing states are shown in Figure 3. As can be seen, when the maximum conductance $g_{kc}$ and the $\lambda_n$ are fixed, the neuron's electrical activities undergo a transition into complex firing modes. First, to characterize the behavior of the firing modes transformation in Figure 2, we plot the action potentials of different parameter areas shown in Figure 3. These results correspond to the bifurcation diagrams.

In addition, in order to investigate the energy computation of neurons in different bursting kinetics, the modes of the action potential of neurons, the electric power of batteries, and the net power $P$ are shown in Figure 4. The electrical power of batteries and net power change as the action potential of neuron firing modes changes, and the electrical power of batteries are very different in value.

### 3.2 Energy efficiency of different bursting kinetics induced by control parameters

In this section, the effects of control parameters ($\lambda_n$, $g_{kc}$, and $k$) on energy are investigated, and it is found that there exists an optimal region of energy efficiency.

To study the system's energy computation and efficiency, we first evaluate the implications of varying the system's maximal conductance. The ratio ($\delta$) is shown in Figure 5(a), whereas the corresponding membrane potential distributions are shown in Figure 5(b). With the maximal conductance increasing, the $E_n$-$E_p$ ratio gradually decreases (while the ratio rapidly changes between 6 and 12 $s^{-1}$), showing that the distribution of membrane potential has significantly changed. The corresponding membrane potential distributions for four special values (purple dots) show that when the maximal conductance increases, the membrane potential distribution changes from mostly above to predominantly below the threshold potential (−46 mV). When $g_{kc}$ = 6.0 $s^{-1}$, the membrane potential of the high-frequency bursting pattern is primarily between −46 and −20 mV and is generally greater than the threshold potential (−46 mV). When $g_{kc}$ = 12.0 $s^{-1}$, the frequency distributed between −46 and −20 mV is significantly reduced, whereas when $g_{kc}$ = 19.5 and 23.6 $s^{-1}$, the membrane potential of the low-frequency bursting pattern is primarily between −60 and −46 mV, which is below the threshold potential. As a result, neurons with a high-fre-

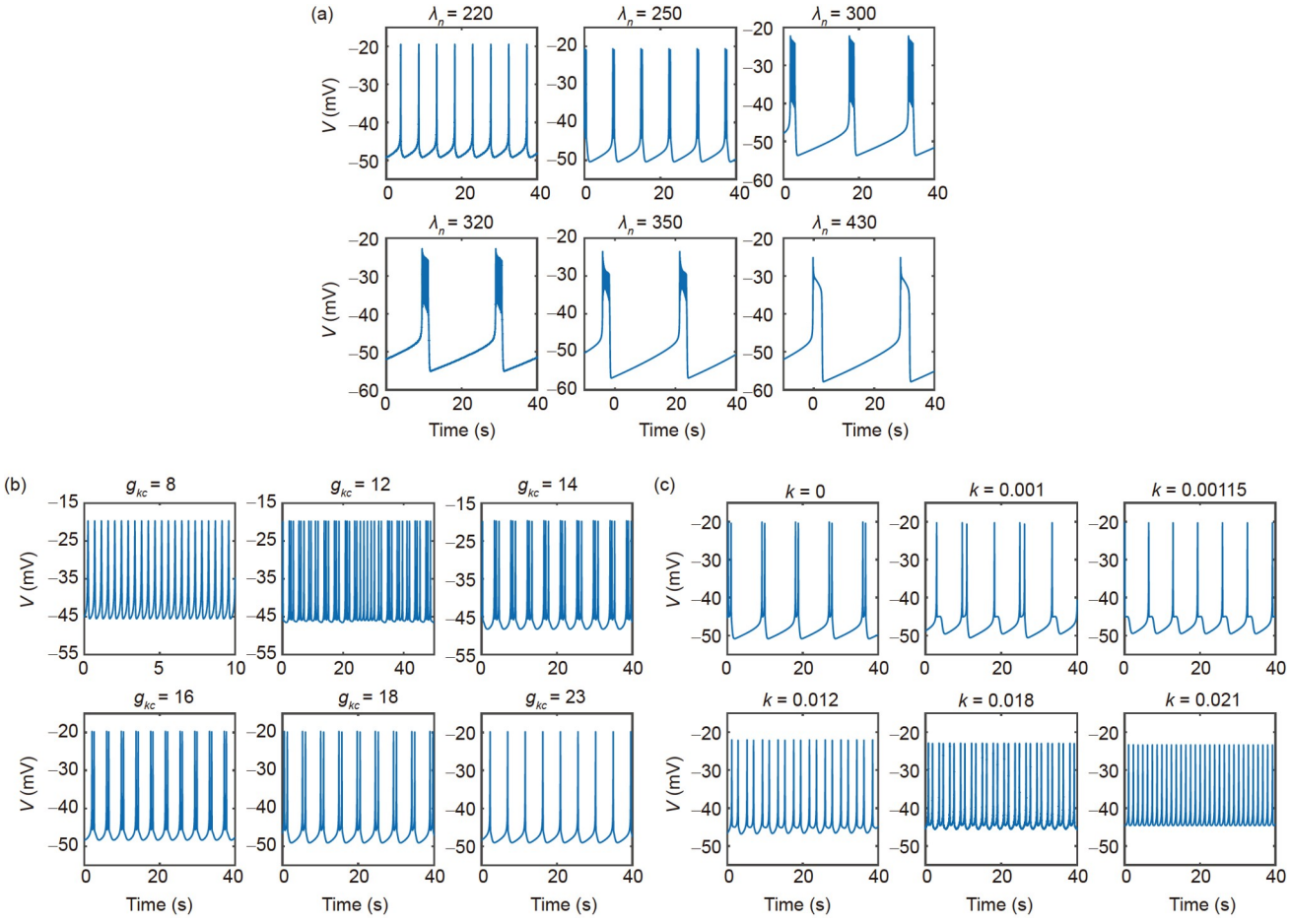


**Figure 3** (Color online) Firing modes of neurons' electrical activities driven by different parameters. The maximal conductance $g_{kc}$ and relaxation time constant $\lambda_n$ are set as $\lambda_n$ = 240.4 and $g_{kc}$ = 23.6 $s^{-1}$.

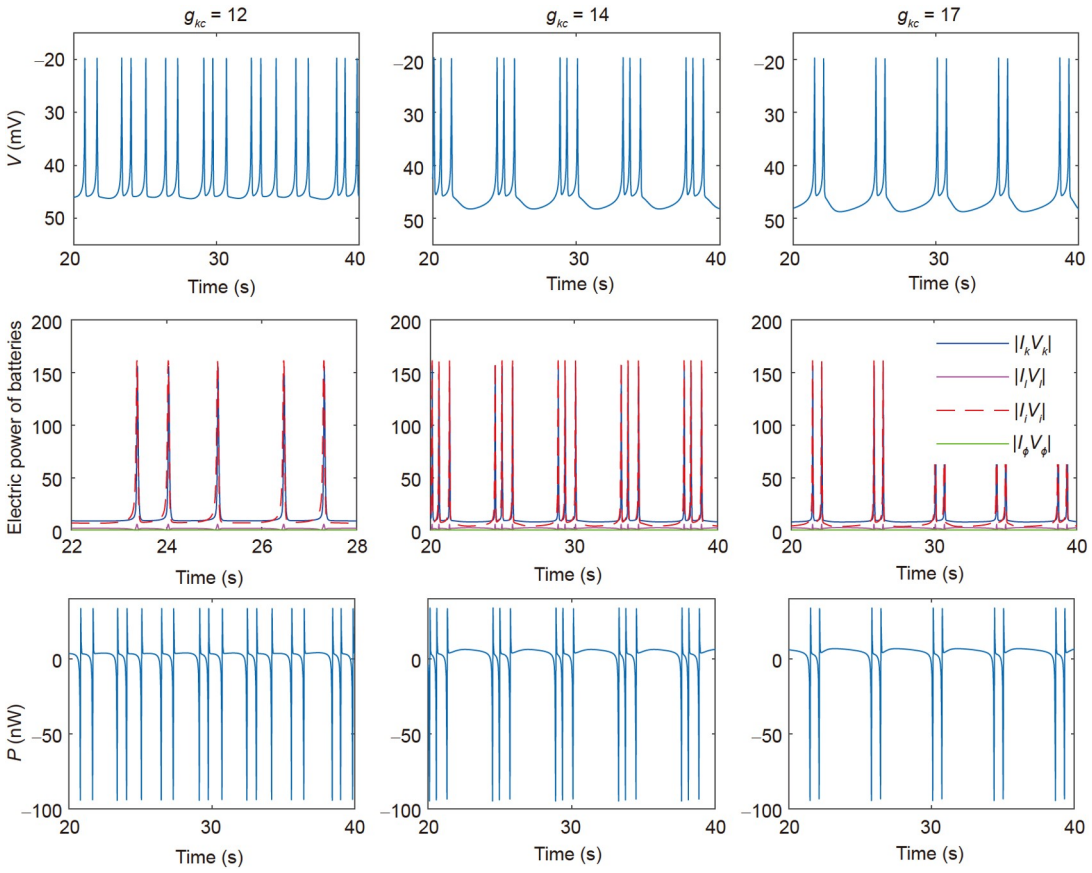


**Figure 4** (Color online) Modes of the neurons' action potential, the electric power of batteries, and the net power $P$ under different parameters. The parameters are set as $k$ = 0.001 and $\lambda_n$ = 230. The larger the value of maximal conductance, the higher the neuron's discharge frequency.

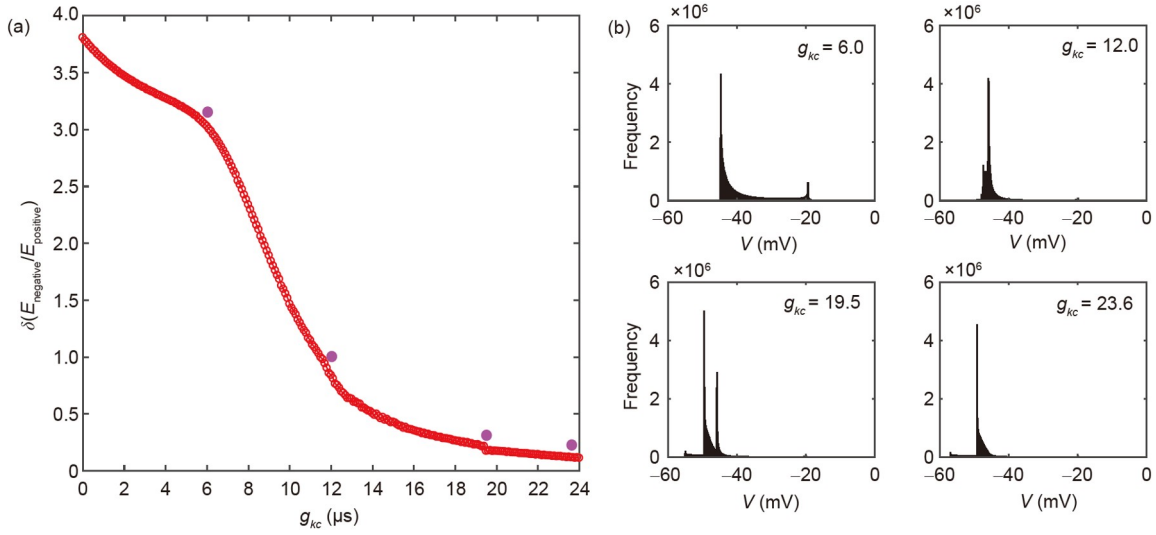


**Figure 5** (Color online) (a) Ratio ($\delta$) of the negative energy consumption to positive energy consumption; (b) membrane potential distribution of various maximal conductances ($g_{kc}$). The parameters are set as $\lambda_n$ = 230 and $k$ = 0.001.

quency burst consume more negative energy than neurons with a low-frequency bursting pattern, which consumes more positive energy.

So as to study the effect of maximal conductance on the energy efficiency of different bursting kinetics, the information ($CV$) and total energy consumption ($E$) are shown in Figure 6(a). When the parameters are fixed as $\lambda_n$ = 230, $k$ = 0.001, and maximal conductance is in the range of 10.35–19.55 $s^{-1}$, the neuron in different period-$n$ bursting states (as shown in Figure 2(b)) carries relatively high

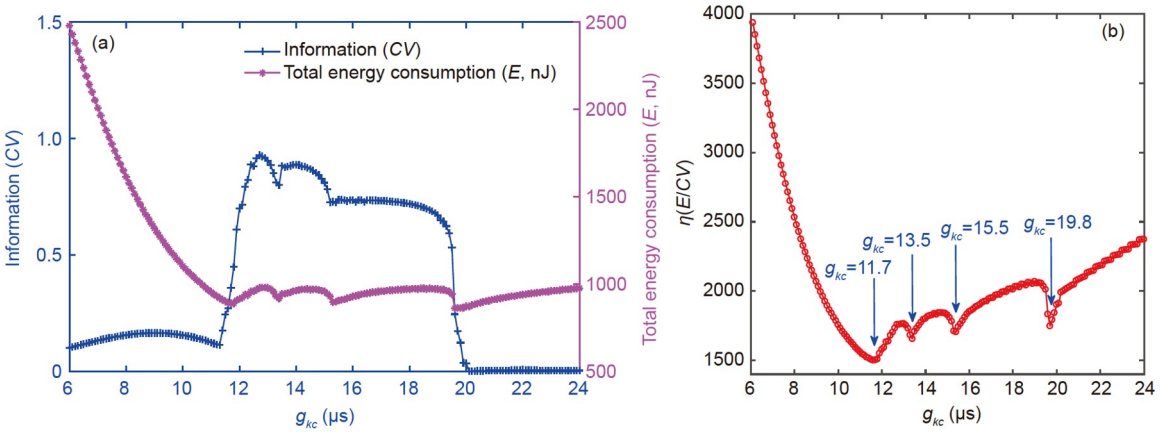


**Figure 6** (Color online) (a) Information and total energy consumption; (b) energy efficiency; a lower $\eta$ value signifies high energy efficiency. The parameters are set as $\lambda_n$ = 230 and $k$ = 0.001.

amounts of information, the neuron in a periodic spiking state carries low amounts of information, and the total energy consumption is relatively low. The extreme points ($g_{kc}$ = 11.7, 13.5, 15.5, 19.8 $s^{-1}$) of the blue line (information) and the purple line (total energy consumption) correspond to the mixed discharge state where the neuron is in several bursting states simultaneously. This is very different from previous work [25]. Under electromagnetic induction, there are several low-value states of energy efficiency that correspond to the mixed discharge state.

Therefore, the energy efficiency calculated (Figure 6(b)) shows that the neuron in different period-$n$ bursting states consumes less energy per unit of information, resulting in higher energy efficiency. In particular, a mixed discharge state where neurons are in several bursting states simultaneously has high energy efficiency. In this condition, the different period-$n$ bursting states belong to a medium-frequency pattern, which reduces energy consumption by producing fewer spikes and consuming the potential energy stored in the ion concentration gradient. On the contrary, the neuron in a periodic spiking state (high-frequency pattern or low-frequency pattern) consumes more energy per unit of information, which means low energy efficiency. The possible reasons for low efficiency are that high-frequency patterns dissipate the energy stored in the $Na^+$ gradient and do not fully dissipate the energy stored in the $K^+$ gradient, resulting in wasted energy. Low-frequency patterns do not fully dissipate the energy stored in the $Na^+$ gradient and excessively dissipate the energy stored in the $K^+$ gradient. Thus, excessive $Na^+$ gradients induce sparse firing, resulting in energy waste in information transmission [56].

In addition, the effects of feedback gain on energy computation and energy efficiency of the neuron system are being studied. The ratio ($\delta$) is computed at different feedback gains in Figure 7(a), and the corresponding membrane potential distributions are shown in Figure 7(b).

With the feedback gain increasing, the $E_n$-$E_p$ ratio first increases, reaches a maximum, and then reduces again. The neuron in low feedback gain (below 0.1) has a low-frequency firing rhythm (the corresponding value of ISI is larger in Figure 2(a)), and the membrane potential of the low-frequency bursting pattern is mostly between −60 and −46 mV, which is below the threshold potential. While the neuron in high feedback gain (above 0.1) has a high-frequency firing rhythm, the membrane potential distribution changes from mostly above the threshold potential (−46 mV) to mostly below the threshold potential. Therefore, a high-frequency pattern of neurons consumes more negative energy than a low-frequency pattern of neurons consumes more positive energy.

Furthermore, the energy efficiency of different firing modes induced by feedback gain is evaluated in Figure 8(b), and the information ($CV$) and total energy consumption ($E$) are shown in Figure 8(a).

First of all, from the overall point of view, the information is in a low value state. Interesting changes (green box) occur when feedback is small and total energy consumption first increases and then decreases. What needs to be emphasized is that as feedback gain increases (green box), the information undergoes a succession: decreases → increases → decreases. That is, the information carried by the neuron in different firing patterns decreases first, then increases, and finally decreases. These results are consistent with the firing state in Figure 2(a). Furthermore, Figure 8(b) shows that when the value $\eta$ remains low, the neuron consumes less energy per unit of information with a lower feedback gain $k$, implying that the neuron in a complex bursting state is highly energy efficient. Therefore, it is found that low feedback current induced by electromagnetic induction can enhance neural energy efficiency. The neuron in a complex period bursting state carries high amounts of information. Total energy consumption is relatively low, and it has high energy efficiency.

The effects of relaxation time constant $\lambda_n$ on energy

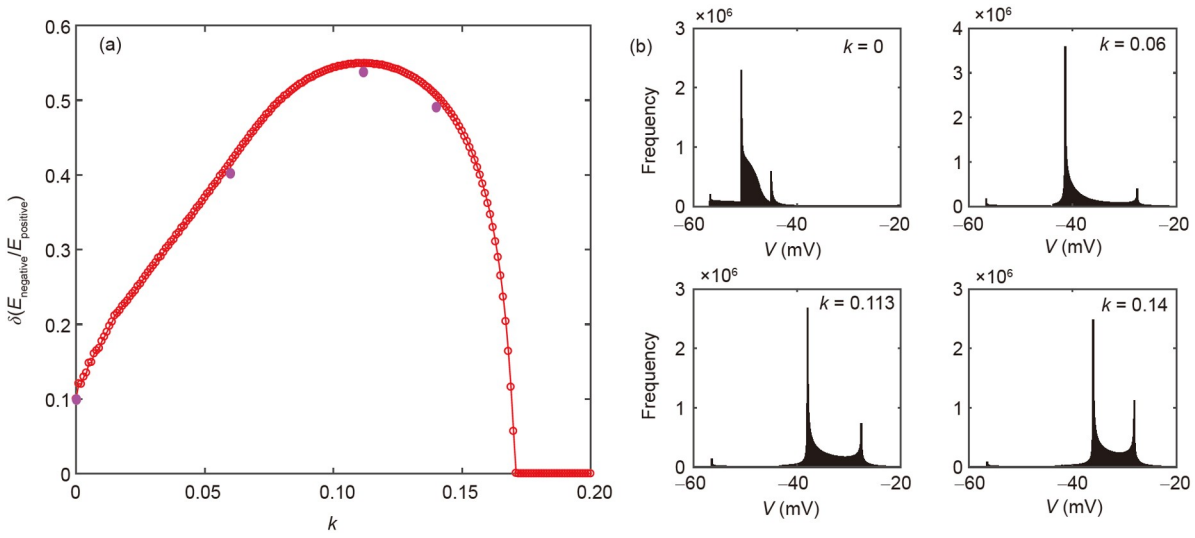


**Figure 7** (Color online) (a) Ratio ($\delta$) of the negative energy consumption to positive energy consumption; (b) membrane potential distribution of various feedback gain $k$. The parameters are set as $\lambda_n$ = 240.4 and $g_{kc}$ = 23.6 s$^{-1}$.

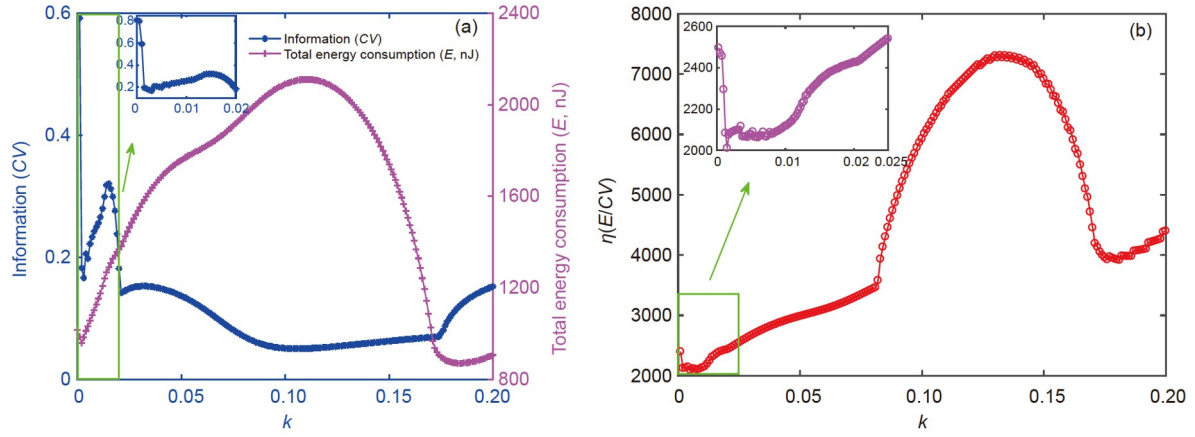


**Figure 8** (Color online) (a) Information and total energy consumption; (b) energy efficiency. The parameters are set as $\lambda_n$ = 240.4 and $g_{kc}$ = 23.6 s$^{-1}$.

computation and energy efficiency of the neuron system are investigated. First, $\delta$ shows obvious fluctuations in Figure 9(a). When the relaxation time constants are small, the membrane voltage of the low-frequency bursting pattern is mostly between −60 and −46 mV, which is below the threshold potential. With the $\lambda_n$ increasing, the $E_n$-$E_p$ ratio gradually decreases; the distribution is that one-third of the membrane potential is above the threshold potential (−46 mV) and nearly two-thirds of the membrane potential is lower than the threshold potential. Thus, the high-frequency bursting pattern of neurons consumes more negative energy than the low-frequency bursting pattern of neurons consumes more positive energy. These results are consistent with the above conclusion.

In addition, the information ($CV$), total energy consumption ($E$), and energy efficiency are calculated in Figure 10. With relaxation time constant increasing, the information undergoes a successive transition, i.e., first maintaining a stable low state → increase → decrease. This transition corresponds to the neuron firing state shown in Figure 2(b). And total energy consumption increases first, then decreases and maintains a stable value. Furthermore, when the parameters are fixed as $g_{kc}$ = 23.6 s$^{-1}$, $k$ = 0.001, and the relaxation time constant is in the range of 240 and 381, the neuron is in a different period-n bursting state (as shown in Figure 2(a)). At this time, the neuron consumes less energy per unit of information in the green box (Figure 6(b)), which means higher energy efficiency.

As a result, it is found that the more complex the state of the neuron, the greater the information ($CV$) and the higher the total energy consumption. However, the neuron in a complex period-$n$ bursting state consumes relatively less energy per unit of information; that is, the neuron in a complex period-$n$ bursting state carries high amounts of information, the total energy consumption is relatively low, and the energy efficiency is high. The different period-$n$ bursting states belong to medium-frequency patterns (as shown in Figure 2(a)), which reduce the energy consumption

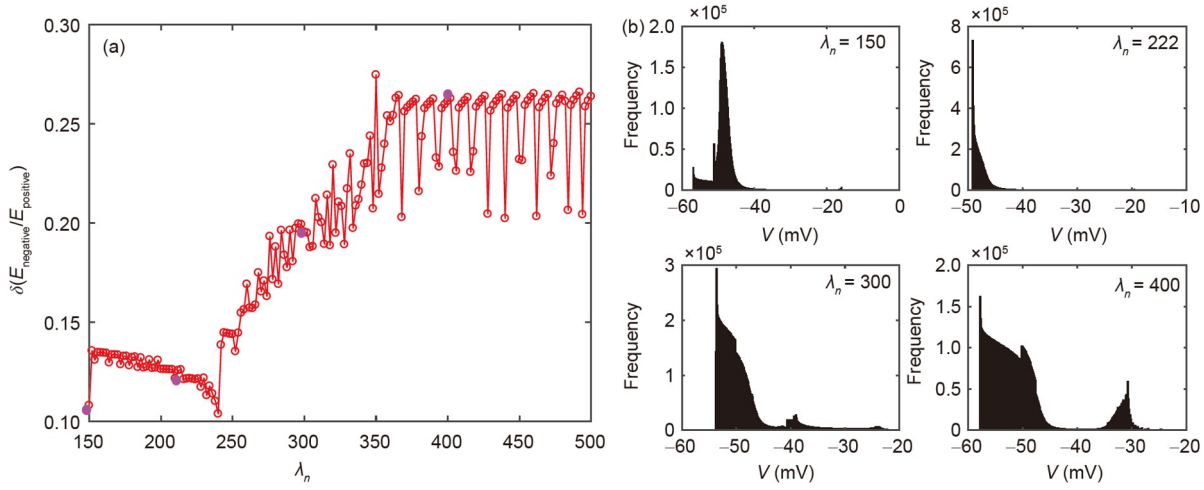


**Figure 9** (Color online) (a) Ratio ($\delta$) of the negative energy consumption to positive energy consumption; (b) membrane potential distribution of various relaxation time constants $\lambda_n$. The parameters are set as $g_{kc}$ = 23.6 $s^{-1}$ and $k$ = 0.001.

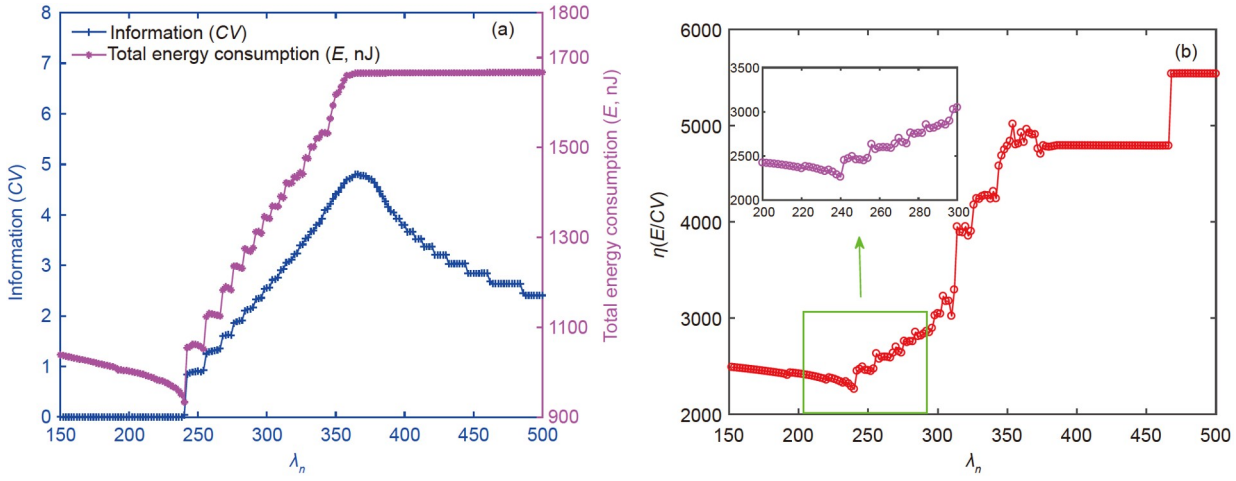


**Figure 10** (Color online) (a) Information and total energy consumption; (b) energy efficiency. The parameters are set as $g_{kc}$ = 23.6 $s^{-1}$ and $k$ = 0.001.

by producing fewer spikes and consuming the potential energy stored in the ion concentration gradient.

### 3.3 Energy efficiency of different bursting kinetics induced by the combined influence of $k$, $g_{kc}$, and $\lambda_n$

In this section, the energy efficiency and the information are discussed under the combined influence of the $\lambda_n$, $g_{kc}$, and $k$. The results show that there is an optimal parameter area where the neuron has high energy efficiency; that is, it carries a high amount of information and consumes less energy.

The combined effect of the relaxation time constant $\lambda_n$ and the maximum conductance $g_{kc}$ are shown in Figure 11. The state of "the middle is high and the ends are gradually decreased" is shown in Figure 11(a). When the relaxation time constant $\lambda_n$ is fixed at 350, the information is relatively large. However, when the maximal conductance $g_{kc}$ is set to a value between 6 and 10 $s^{-1}$, the information greatly fluctuates. There exists an intermediate area of maximal conductance the relaxation time constant is fixed, the information is larger, and the neuron carries a high amount of information. The total energy consumption shown in Figure 11(b) is a "step" style change; at a lower relaxation time constant and median of maximal conductance (from 10 to 20 $s^{-1}$), the neuron consumes relatively low total energy.

The reciprocal of the $1/\eta$ value is shown in Figure 11(c); the change trend of $1/\eta$ is opposite to that of Figure 6(b) and Figure 10(b). A bigger $1/\eta$ value shows higher energy efficiency (that is, lower energy consumption per unit of information). It has been observed that an obvious area with a high $1/\eta$ value exists in which the neuron carries a large amount of information while consuming less energy. In addition, the ratio ($\delta$) is shown in Figure 10(d). At a low maximal conductance and high relaxation time constant, the neuron is in a high-frequency bursting pattern, the $E_n$-$E_p$ ratio is high, and the neuron consumes more negative energy. On

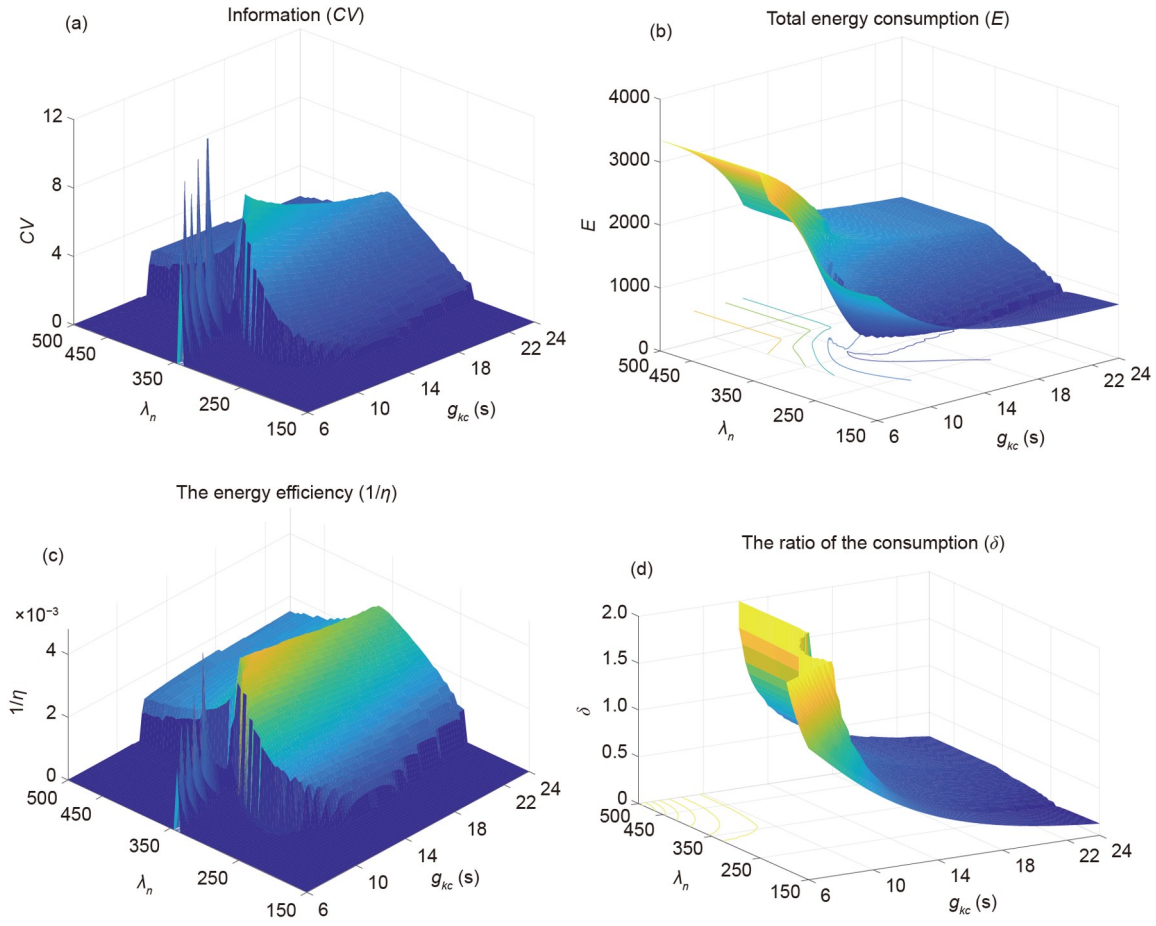


**Figure 11** (Color online) (a) Information (*CV*); (b) total energy consumption (*E*, nJ); (c) energy efficiency; (d) ratio ($\delta$) of the negative to positive energy consumption. The value of the parameter is set to $k = 0.001$.

the contrary, when the neuron has a high maximal conductance and a short relaxation time constant, it bursts at a low frequency, the $E_n$-$E_p$ ratio is low, and the neuron consumes more positive energy.

Thus, a neuron with a high-frequency bursting pattern consumes more negative energy, whereas a neuron with a low-frequency bursting pattern consumes more positive energy. Additionally, there is an optimal parameter area of maximum conductance and relaxation time constant where the energy efficiency of firing modes is greatest, and the neuron carries a large amount of information while consuming less energy per unit of information.

Furthermore, the combined influences of feedback gain $k$ and relaxation time constant $\lambda_n$ on energy efficiency are shown in Figure 12. The information in Figure 12(a) presents an obvious high-low distribution; it is found that the information (*CV*) is larger at a high relaxation time constant, shows an obvious high distribution, and carries high amounts of information at high feedback gain and high relaxation time constant. The total energy consumption in Figure 12(b) also shows a "step" style change; as we can see, the neuron consumes relatively low total energy at high feedback gain and high relaxation time constant. On the contrary, at higher feedback gain (0.05–0.1) and lower relaxation time constant (150–240), the neuron consumes relatively high total energy.

In addition, the reciprocal of the $1/\eta$ value is calculated in Figure 12(c); it is observed that there exists a high $1/\eta$ value area of the high feedback gain and high the relaxation time constant, in which the neuron carried high amounts of information, but consumes less energy. In addition, the ratio ($\delta$) is shown in Figure 12(d). The $E_n$-$E_p$ ratio shows a "step" style change, and if it is below 0.6, the neuron consumes more positive energy than negative energy.

Additionally, under the combined influence of feedback gain $k$ and maximal conductance $g_{kc}$ in Figure 13. The information in Figure 13(a) presents the obvious protrusion, i.e., under the lower feedback gain ($0 < k < 0.02$) and the intermediate maximal conductance ($12\ s^{-1} < g_{kc} < 20\ s^{-1}$), the information is relatively large, and the neuron carried high amounts of information. The total energy consumption in Figure 13(b) shows the smooth change; it is found that under the lower feedback gain, the neuron consumes relatively low total energy.

The reciprocal of the $1/\eta$ value is shown in Figure 13(c). There is a high $1/\eta$ value area of lower feedback gain ($0 < k < 0.02$) and an intermediate maximal conductance ($12\ s^{-1} < g_{kc}$

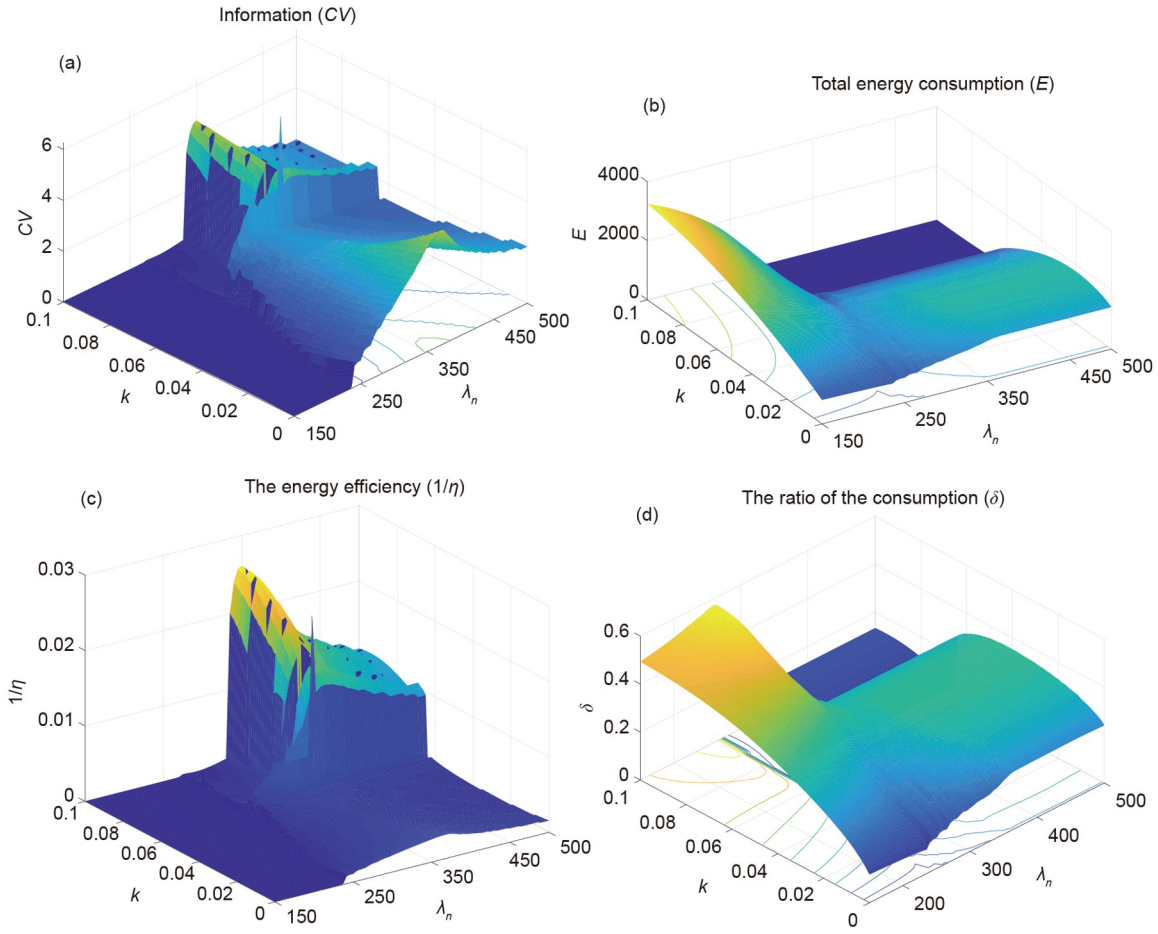


**Figure 12** (Color online) (a) Information (*CV*); (b) total consumption (*E*, nJ); (c) energy efficiency; (d) ratio ($\delta$) of the negative energy consumption to positive energy consumption. The parameter is set as $g_{kc}$ = 23.6 $s^{-1}$.

< 20 $s^{-1}$), in which the neuron carries high amounts of information but consumes less energy. The ratio ($\delta$) is shown in Figure 13(d). Under the high maximal conductance and lower feedback gain, the neuron is in a period-*n* bursting pattern, the $E_n$-$E_p$ ratio is low, and the neuron consumes more positive energy. On the contrary, under the lower maximal conductance and high feedback gain, the neuron is in a spiking pattern, the $E_n$-$E_p$ ratio is high, and the neuron consumes more negative energy.

As a result, the period-*n* bursting pattern of a neuron consumes more positive energy than the spiking pattern of a neuron consumes more negative energy. And there exists the optimal parameter area of maximal conductance and feedback gain, where the energy efficiency of firing modes is greatest, and the neuron carries high amounts of information and consumes less energy per unit of information.

## 4 Conclusions and discussion

Neural information encoding takes place in firing sequences; neurons carry different amounts of information in different firing patterns [23,49,57]. The firing patterns will consume a significant amount of energy during the transition process, but the firing pattern of the nervous system determines energy efficiency is unclear. As a result, it is necessary to study the energy consumption and efficiency of neurons and neuron systems in different firing patterns and modes of transformation.

The energy-efficiency firing modes of different bursting kinetics are investigated using the Chay neuron model. First, we studied the complex firing modes of neurons and found that as the time constant $\lambda_n$ increases, the neuron experiences the complex bursting kinetics with tuning system parameter with the time constant $\lambda_n$ increasing, the dynamic transition experiences a succession: spiking state → period-2 bursting state → period-3 bursting state → period-4 bursting state → period-*n* bursting state → spiking state. When the maximal conductances of $g_{kc}$ are increased, an interesting transformation occurs in the firing modes: spiking state → closed period-*n* bursting state → period-4 bursting state → period-3 bursting state → period-2 bursting state → spiking state. Furthermore, the complex bifurcation process with respect to feedback gains *k* is: period-2 bursting state → spiking state → period-2 bursting state → spiking state. Compared with

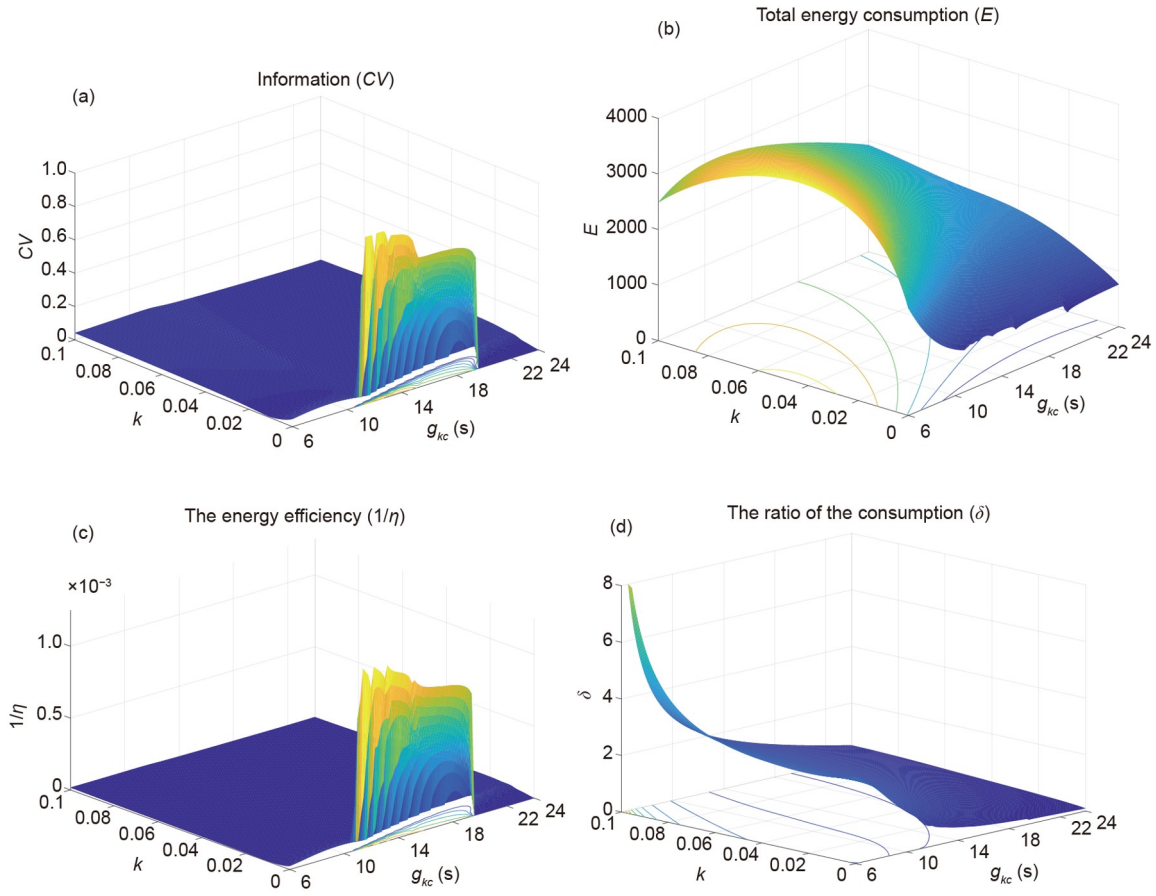


**Figure 13** (Color online) (a) Information (*CV*); (b) total consumption (*E*, nJ); (c) energy efficiency; (d) ratio ($\delta$) of the negative energy consumption to positive energy consumption. The parameter is set as $\lambda_n = 230$.

the previous work [25], the discharge activity of neurons induced by electromagnetic induction becomes more complex, with the appearance of a mixed discharge state where the neuron is simultaneously in several bursting states.

Following that, the relationship between energy consumption and information is discussed. (1) While neurons with a high-frequency bursting pattern consume more negative energy, neurons with a low-frequency pattern consume more positive energy. (2) At an intermediate maximal conductance $g_{kc}$ (10.35–19.55 $s^{-1}$), the neuron is in a different period-*n* bursting state, consuming less energy per unit of information, demonstrating a higher energy efficiency. On the contrary, when a neuron is in a periodic spiking state, it consumes more energy per unit of information, which means lower energy efficiency. Additionally, there are several states with extremely low energy efficiency, which correspond to a mixed discharge state, where neurons are in several bursting states simultaneously. (3) Neural energy efficiency can be enhanced when a low feedback current is induced by electromagnetic induction ($k$ = 0.0115–0.0206). The neuron in a complex period bursting state carries a high amount of information, total energy consumption is relatively low, and energy efficiency is high. (4) When the relaxation time constant is between 240 and 381, the neuron is in a different period-*n* bursting state. At this time, the neuron in a complex period-*n* bursting state carries a high amount of information, total energy consumption is relatively low, and it has high energy efficiency. (5) The period-*n* bursting state (medium-frequency patterns) induced by an appropriate control parameter demonstrates more efficient use of sodium entry due to the reduced overlap load between the inward $Na^+$ and outward $K^+$ currents [35,56].

Finally, the effects of control parameters ($\lambda_n$, $g_{kc}$, and $k$) on energy consumption and efficiency are studied. It is found that there are optimal system parameters where the energy efficiency of firing modes is greatest, and the neuron may carry a high amount of information while consuming less energy per unit of information.

The study contributes to the understanding of the energy mechanism of neural information propagation and sheds light on the energy efficiency of neuron systems. It is necessary to continue studying the relationship between the complex discharge mode and energy efficiency of the noise neuron system with time delay, as well as to discuss the relationship between signal propagation and energy in multilayer neural systems.

*This work was supported by the National Natural Science Foundation of China (Grant No. 11675060) and the China Postdoctoral Science Foundation (Grant No. 2021M703011).*


1 Fu X, Yu Y. Reliable and efficient processing of sensory information at body temperature by rodent cortical neurons. Nonlinear Dyn, 2019, 98: 215–231
2 Yue Y, Liu L, Liu Y, et al. Dynamical response, information transition and energy dependence in a neuron model driven by autapse. Nonlinear Dyn, 2017, 90: 2893–2902
3 Yu L, Yu Y. Energy-efficient neural information processing in individual neurons and neuronal networks. J Neurosci Res, 2017, 95: 2253–2266
4 Jha M K, Morrison B M. Glia-neuron energy metabolism in health and diseases: New insights into the role of nervous system metabolic transporters. Exp Neurol, 2018, 309: 23–31
5 Lu L, Jia Y, Kirunda J B, et al. Effects of noise and synaptic weight on propagation of subthreshold excitatory postsynaptic current signal in a feed-forward neural network. Nonlinear Dyn, 2019, 95: 1673–1686
6 Ge M, Jia Y, Lu L, et al. Propagation characteristics of weak signal in feedforward izhikevich neural networks. Nonlinear Dyn, 2020, 99: 2355–2367
7 Wang R, Fan Y C, Wu Y. Spontaneous electromagnetic induction promotes the formation of economical neuronal network structure via self-organization process. Sci Rep, 2019, 9: 9698
8 Xu Y, Guo Y, Ren G, et al. Dynamics and stochastic resonance in a thermosensitive neuron. Appl Math Comput, 2020, 385: 125427
9 Yao Y, Ma J. Logical chaotic resonance in a bistable system. Int J Bifurcat Chaos, 2020, 30: 2050196
10 Yao Y, Ma J, Gui R, et al. Enhanced logical chaotic resonance. Chaos, 2021, 31: 023103
11 Zhu Z, Ren G, Zhang X, et al. Effects of multiplicative-noise and coupling on synchronization in thermosensitive neural circuits. Chaos Soliton Fract, 2021, 151: 111203
12 Danziger Z, Grill W M. A neuron model of stochastic resonance using rectangular pulse trains. J Comput Neurosci, 2015, 38: 53–66
13 Vilar J M G, Rubí J M. Noise suppression by noise. Phys Rev Lett, 2001, 86: 950–953
14 Shimokawa T, Pakdaman K, Sato S. Time-scale matching in the response of a leaky integrate-and-fire neuron model to periodic stimulus with additive noise. Phys Rev E, 1999, 59: 3427–3443
15 Lu L, Jia Y, Ge M, et al. Inverse stochastic resonance in hodgkin-huxley neural system driven by gaussian and non-gaussian colored noises. Nonlinear Dyn, 2020, 100: 877–889
16 Li Y, Wei Z, Zhang W, et al. Bogdanov-Takens singularity in the hindmarsh-rose neuron with time delay. Appl Math Comput, 2019, 354: 180–188
17 Wang G, Yu D, Ding Q, et al. Effects of electric field on multiple vibrational resonances in hindmarsh-rose neuronal systems. Chaos Solitons Fractals, 2021, 150: 111210
18 Lin H, Wang C. Influences of electromagnetic radiation distribution on chaotic dynamics of a neural network. Appl Math Comput, 2020, 369: 124840
19 Izhikevich E M. Which model to use for cortical spiking neurons? IEEE Trans Neural Netw, 2004, 15: 1063–1070
20 Steriade M, Nunez A, Amzica F. A novel slow (<1 Hz) oscillation of neocortical neurons *in vivo*: Depolarizing and hyperpolarizing components. J Neurosci, 1993, 13: 3252–3265
21 Hunt D L, Lai C, Smith R D, et al. Multimodal *in vivo* brain electrophysiology with integrated glass microelectrodes. Nat Biomed Eng, 2019, 3: 741–753
22 Barral J, Wang X J, Reyes A D. Propagation of temporal and rate signals in cultured multilayer networks. Nat Commun, 2019, 10: 3969
23 Strong S P, Koberle R, de Ruyter van Steveninck R R, et al. Entropy and information in neural spike trains. Phys Rev Lett, 1998, 80: 197–200
24 Jia Y, Gu H. Identifying nonlinear dynamics of brain functional networks of patients with schizophrenia by sample entropy. Nonlinear Dyn, 2019, 96: 2327–2340
25 Zhu F, Wang R, Aihara K, et al. Energy-efficient firing patterns with sparse bursts in the chay neuron model. Nonlinear Dyn, 2020, 100: 2657–2672
26 Zhou S L, Yu Y G. Synaptic EI balance underlies efficient neural coding. Front Neurosci, 2018, 12: 45–46
27 Zaks M A, Sailer X, Schimansky-Geier L, et al. Noise induced complexity: From subthreshold oscillations to spiking in coupled excitable systems. Chaos, 2005, 15: 026117
28 Trang-Anh N, Bartosz T, Olivier M, et al. Maximum-entropy models reveal the excitatory and inhibitory correlation structures in cortical neuronal activity. Phys Rev E, 2018, 98: 012402
29 Yang H H, Amari S. Adaptive online learning algorithms for blind separation: Maximum entropy and minimum mutual information. Neural Comput, 1997, 9: 1457–1482
30 Kamimura R. Mutual information maximization for improving and interpreting multi-layered neural networks. In: 2017 IEEE Symposium Series on Computational Intelligence (SSCI). Honolulu, 2017
31 Xu L, Qi G, Ma J. Modeling of memristor-based hindmarsh-rose neuron and its dynamical analyses using energy method. Appl Math Model, 2022, 101: 503–516
32 Lu L L, Jia Y, Xu Y, et al. Energy dependence on modes of electric activities of neuron driven by different external mixed signals under electromagnetic induction. Sci China Tech Sci, 2019, 62: 427–440
33 Zhou P, Hu X, Zhu Z, et al. What is the most suitable lyapunov function? Chaos Soliton Fract, 2021, 150: 111154
34 Wang Y, Xu X, Wang R. The place cell activity is information-efficient constrained by energy. Neural Networks, 2019, 116: 110–118
35 Sengupta B, Stemmler M, Laughlin S B, et al. Action potential energy efficiency varies among neuron types in vertebrates and invertebrates. PLoS Comput Biol, 2010, 6: e1000840
36 Oh S, Shi Y, Del Valle J, et al. Energy-efficient Mott activation neuron for full-hardware implementation of neural networks. Nat Nanotechnol, 2021, 16: 680–687
37 Yu L, Shen Z, Wang C, et al. Efficient coding and energy efficiency are promoted by balanced excitatory and inhibitory synaptic currents in neuronal network. Front Cell Neurosci, 2018, 12: doi: 10.3389/fncel.2018.00123
38 Zhu F, Wang R, Pan X, et al. Energy expenditure computation of a single bursting neuron. Cogn Neurodyn, 2019, 13: 75–87
39 Bélanger M, Allaman I, Magistretti P J. Brain energy metabolism: Focus on astrocyte-neuron metabolic cooperation. Cell Metab, 2011, 14: 724–738
40 Usha K, Subha P A. Collective dynamics and energy aspects of star-coupled hindmarsh-rose neuron model with electrical, chemical and field couplings. Nonlinear Dyn, 2019, 96: 2115–2124
41 Du M, Li J, Wang R, et al. The influence of potassium concentration on epileptic seizures in a coupled neuronal model in the hippocampus. Cogn Neurodyn, 2016, 10: 405–414
42 Li J, Tang J, Ma J, et al. Dynamic transition of neuronal firing induced by abnormal astrocytic glutamate oscillation. Sci Rep, 2016, 6: 32343
43 Zare M, Zafarkhah E, S. Anzabi-Nezhad N. An area and energy efficient LIF neuron model with spike frequency adaptation mechanism. Neurocomputing, 2021, 465: 350–358
44 Das B, Schulze J, Ganguly U. Ultra-low energy LIF neuron using Si NIPIN diode for spiking neural networks. IEEE Electron Device Lett, 2018, 39: 1832–1835
45 Peng Z X, Wang J P, Zhan Y, et al. A high-accuracy and energy-efficient CORDIC based izhikevich neuron. In: 2021 19th IEEE International New Circuits and Systems Conference (NEWCAS). Toulon, 2021
46 He Z Z, Fan D L. A tunable magnetic skyrmion neuron cluster for energy efficient artificial neural network. In: Design, Automation & Test in Europe Conference & Exhibition (DATE). Lausanne, 2017
47 Cruz-Albrecht J M, Yung M W, Srinivasa N. Energy-efficient neuron,

synapse and STDP integrated circuits. IEEE Trans Biomed Circuits Syst, 2012, 6: 246–256
48 Dienel G A, Rothman D L. Reevaluation of astrocyte-neuron energy metabolism with astrocyte volume fraction correction: Impact on cellular glucose oxidation rates, glutamate-glutamine cycle energetics, glycogen levels and utilization rates vs. Exercising muscle, and $Na^+$/$K^+$ pumping rates. Neurochem Res, 2020, 45: 2607–2630
49 Alle H, Roth A, Geiger J R P. Energy-efficient action potentials in hippocampal mossy fibers. Science, 2009, 325: 1405–1408
50 Litt B, Esteller R, Echauz J, et al. Epileptic seizures may begin hours in advance of clinical onset. Neuron, 2001, 30: 51–64
51 Zhu Z, Wang R, Zhu F. The energy coding of a structural neural network based on the hodgkin-huxley model. Front Neurosci, 2018, 12: 122–137
52 Wang Q, Ma X, Wang H. Information processing and energy efficiency of temperature-sensitive morris-lecar neuron. Biosystems, 2020, 197: 104215
53 Wu K J, Yu C, Wang D C. The dynamics behaviors of Chay neuron model under different parameters. Concurr Comp Pract Exper, 2019, 31: e4836
54 Wu F, Wang C, Jin W, et al. Dynamical responses in a new neuron model subjected to electromagnetic induction and phase noise. Physica A, 2017, 469: 81–88
55 Moujahid A, d'Anjou A, Torrealdea F J, et al. Energy and information in hodgkin-huxley neurons. Phys Rev E, 2011, 83: 031912
56 Carter B C, Bean B P. Sodium entry during action potentials of mammalian neurons: Incomplete inactivation and reduced metabolic efficiency in fast-spiking neurons. Neuron, 2009, 64: 898–909
57 Denève S, Machens C K. Efficient codes and balanced networks. Nat Neurosci, 2016, 19: 375–382